

Properties of Planet-induced Deviations in the Astrometric Microlensing Centroid Shift Trajectory

Cheongho Han[†] & Chunguk Lee^{‡*}

[†]*Department of Physics, Chungbuk National University, Chongju 361-763, Korea*

[‡]*Department of Astronomy & Space Science, Chungbuk National University, Chongju 361-763, Korea*

13 June 2021

ABSTRACT

An extra-solar planet can be detected by microlensing because it can distort the smooth lensing light curve created by the primary lens. As a new method to search for and characterize extra-solar planets, Safizadeh, Dalal & Griest proposed to detect the planet-induced distortions in the trajectory of the microlensed source star's centroid motion (astrometric curve), which is observable by using the next generation of high-precision interferometers. In this paper, we investigate the properties of the planet-induced deviations in the astrometric curves (excess centroid shifts $\Delta\delta$) and the correlations of $\Delta\delta$ with the photometric deviations. For this, we construct vector field maps of $\Delta\delta$, which represent the difference of the centroid shift from that expected in the absence of the planet as a function of source positions. From this investigation, we find that significant astrometric deviations occur not only in the region near the caustics but also in the region close to the planet-primary axis between the caustics. However, due to the difference in the locations of the caustics between the two types of systems with the planet-primary separations (normalized by the angular Einstein ring radius) $u_p > 1.0$ and $u_p < 1.0$, the locations of the major deviation regions of the two systems are different each other. For systems with $u_p > 1.0$, the major deviation vectors have orientations, in most cases, pointing towards the planet, while they point away from the planet for systems with $u_p < 1.0$. The major deviation region is surrounded by the region of moderate deviations, within which the orientation of $\Delta\delta$ is reversed compared to the orientation in the major deviation region. We also find that the astrometric deviation is closely correlated with the photometric one as discussed by Safizadeh et al. The astrometric deviation increases as the photometric deviation increases and $\Delta\delta$ is directed towards the planet when the light curve has positive deviation and vice versa. We also present excess centroid shift maps for lens systems with various values of the planetary separation, planet/primary mass ratio, and source size to show the changes in the pattern of $\Delta\delta$ with these parameters.

Key words: gravitational lensing – planets and satellites: general

1 INTRODUCTION

Although microlensing was originally proposed by Paczyński (1986) as a method to detect Massive Astrophysical Compact Halo Objects (MACHOs), it can also be used in various other fields of astronomy. One important application is searching for extra-solar planets. Photometrically, planets can be found via the distortions they create in the lensing light curve compared to the smooth and symmetric one of a single lens event (Mao & Paczyński

* e-mails: cheongho@astroph.chungbuk.ac.kr (CH); leecu@astro.chungbuk.ac.kr (LC)

1991; Gould & Loeb 1992; Bolatto & Falco 1994; Wambsganss 1997). Due to the short duration (\mathcal{O} hour – \mathcal{O} day) of the planet-induced deviations, it is difficult to detect them from survey type experiments (e.g., OGLE: Udalski et al. 1993; MACHO: Alcock et al. 1993; EROS: Aubourg et al. 1993; DUO: Alard & Guibert 1997). However, with sufficiently frequent and accurate observations from follow-up monitoring of ongoing events alerted by the survey experiments, it is possible to detect such perturbations and characterize the mass ratio and the projected separation of the planet. Currently, several groups are carrying out such observations (MPS: Rhie et al. 2000; PLANET: Albrow et al. 1998; MOA: Bond 2000).

It was recently shown by Safizadeh, Dalal & Griest (1999) that planets can also be detected from astrometric follow-up observations of lensing events by using the next generation of high-precision interferometers such as the *Space Interferometry Mission* (SIM, Unwin et al. 1997) and those to be mounted on the Keck (Colavita et al. 1998) and the VLT (Mariotti et al. 1998). Precise astrometry using these interferometers will permit measurements of the displacements in the source star image center of light with respect to its un-lensed position, $\boldsymbol{\delta}$ (Miyamoto & Yoshii 1995; Hög, Novikov, & Polnarev 1995; Walker 1995; Boden, Shao, & Van Buren 1998; Miralda-Escudé 1996; Paczyński 1998). The trajectory of the light centroid shifts (astrometric curve) caused by a single point mass is an ellipse (Walker 1995; Jeong, Han & Park 1999). A planet can be detected because it can distort the elliptical astrometric curve of the single lens event, which is analogous to the deviation in the light curve.

In this paper, we investigate the properties of the planet-induced deviations in the astrometric curves. For this, we construct a vector field map of the excess centroid shift $\Delta\boldsymbol{\delta}$, which represents the difference of $\boldsymbol{\delta}$ from that expected in the absence of the planet as a function of source positions. With the map, we examine in detail the correlations between the astrometric and photometric deviations, which were briefly discussed by Safizadeh et al. (1992).

2 BASICS OF MICROLENSING

If a source located at $\boldsymbol{\theta}_S$ is gravitationally lensed by a coplanar N point-mass lens system, where the individual masses and locations are m_j and $\boldsymbol{\theta}_{L,j}$, the positions of the resulting images $\boldsymbol{\theta}$ are obtained by solving the lens equation of the form

$$\boldsymbol{\theta}_S = \boldsymbol{\theta} - \frac{\theta_E^2}{m} \sum_{j=1}^N m_j \frac{\boldsymbol{\theta} - \boldsymbol{\theta}_{L,j}}{|\boldsymbol{\theta} - \boldsymbol{\theta}_{L,j}|^2}, \quad (1)$$

where $m = \sum_{j=1}^N m_j$ is the total mass of the lens system and θ_E is the angular Einstein ring radius. The Einstein ring radius is related to the physical parameters of the lens system by

$$\theta_E = \sqrt{\frac{4Gm}{c^2}} \left(\frac{1}{D_{OL}} - \frac{1}{D_{OS}} \right)^{1/2}, \quad (2)$$

where D_{OL} and D_{OS} represent the distances to the lens and source from the observer, respectively.

For the case of a single point-mass lens ($N = 1$), there are two solutions (and thus the same number of images) of the lens equation and the resulting total magnification and the centroid shift vector take the simple forms

$$A = \frac{u^2 + 2}{u\sqrt{u^2 + 4}}, \quad (3)$$

$$\boldsymbol{\delta} = \frac{\mathbf{u}}{u^2 + 2} \theta_E, \quad (4)$$

where $\mathbf{u} = (\boldsymbol{\theta}_S - \boldsymbol{\theta}_L)/\theta_E$ is the dimensionless lens-source separation vector normalized by θ_E . The separation vector is related to the single lensing parameters by

$$\mathbf{u} = \left(\frac{t - t_0}{t_E} \right) \hat{\mathbf{x}} \pm \beta \hat{\mathbf{y}}, \quad (5)$$

where t_E is the Einstein ring radius crossing time (Einstein time scale), β is the closest lens-source separation (impact parameter), t_0 is the time at the moment of the closest approach, and the unit vectors $\hat{\mathbf{x}}$ and $\hat{\mathbf{y}}$ are parallel and normal to the direction of the lens-source transverse motion, respectively. Note that the sign ‘ \pm ’ is used because β is positive definitive.

The lens system with a planet is described by the formalism of the binary lens system (i.e., $N = 2$) with a very low mass companion. For this case, the lens equation becomes a fifth degree polynomial equation (Witt & Mao 1995) and there are three or five solutions (images) depending on the source position with respect to the lenses. The magnifications of the individual images are given by the Jacobian of the transformation (1) evaluated at the image position, i.e.

$$A_i = \left(\frac{1}{|\det J|} \right)_{\boldsymbol{\theta}=\boldsymbol{\theta}_i}; \quad \det J = \left| \frac{\partial \boldsymbol{\theta}_S}{\partial \boldsymbol{\theta}} \right|. \quad (6)$$

Then, the total magnification is given by the sum of the magnifications of the individual images, i.e. $A = \sum_{i=1}^{N_I} A_i$, where N_I is the total number of images. Since the position of the image centroid, $\boldsymbol{\theta}_c$, equals the magnification weighted mean position of the individual images, the source image centroid shift with respect to the unlensed source position is computed by

$$\boldsymbol{\delta} = \boldsymbol{\theta}_c - \boldsymbol{\theta}_S; \quad \boldsymbol{\theta}_c = \frac{\sum_i^{N_I} A_i \boldsymbol{\theta}_i}{A}. \quad (7)$$

The fundamental difference in the geometry of a binary lens system from that of a single point-mass lens is the formation of caustics. The caustics are the set of source positions at which the magnification of a point source diverges in the geometric optics limit, i.e. $\det J = 0$. Hence, the most significant planet-induced deviations both in the light and astrometric curves occur when the source passes the region close to the caustics. The set of caustics form closed curves. The maximum size of the caustics occurs when the planet is located in the lensing zone of $0.6 \lesssim u_p \lesssim 1.6$ (Gould & Loeb 1992), where u_p is the projected primary-planet separation in units of θ_E (planetary separation).

3 MAPS OF THE EXCESS CENTROID SHIFTS

We investigate the properties of planet-induced deviations in the astrometric curves by constructing maps of excess centroid shifts. The excess centroid shift is defined by

$$\Delta \boldsymbol{\delta} = \boldsymbol{\delta}_p - \boldsymbol{\delta}, \quad (8)$$

where $\boldsymbol{\delta}_p$ and $\boldsymbol{\delta}$ represent the centroid shifts with the presence and absence of the planet, respectively. Therefore, the excess centroid shift vector tells us how much the astrometric curve of an event caused by a lens system with a planet deviates from the elliptical one of a single point-mass event and in which direction the deviation is directed. The excess centroid shift map is analogous to the excess magnification map that was often used to estimate the probability of photometric planet detections (Gould & Loeb 1992; Gaudi & Gould 1997; Gaudi & Sackett 2000). The excess magnification is defined by

$$\epsilon = \frac{A_p - A}{A}, \quad (9)$$

where A_p and A are the magnifications with and without the planet, respectively. We note, however, that $\Delta\boldsymbol{\delta}$ is a vector quantity, while ϵ is a scalar quantity. Hence the excess centroid shift map is a vector field map. With the map, one can obtain an overview of the astrometric behaviors of planet-induced perturbations of all events caused by a lens system, without testing their individual astrometric curves (Han 2001). For the construction of the map, the excess centroid shift on each source position is determined by calculating $\boldsymbol{\delta}$ and $\boldsymbol{\delta}_p$. We calculate $\boldsymbol{\delta}_p$ by numerically solving the binary lens equation, i.e. by solving the fifth degree polynomial equation (Witt & Mao 1995).

4 THE PROPERTIES OF EXCESS CENTROID SHIFTS

As will be shown in the following subsections, the properties of astrometric perturbations are greatly different between the systems with $u_p > 1.0$ and $u_p < 1.0$. Hence, we separately investigate the properties of $\Delta\boldsymbol{\delta}$ for these two types of systems.

4.1 Planets with $u_p > 1.0$

For this type of lens system, there exist two disconnected sets of caustics. One is located near the center of mass (central caustic) and the other caustic (planetary caustic) is located between the primary and the planet (Griest & Safizadeh 1998; Bozza 1999).

In the upper panel of Figure 1, we present the excess centroid shift map of an example lens system composed of a planet with $u_p > 1.0$. The grey-scales in the map are used to represent the regions of significant deviations with $\Delta\delta \geq 0.1\theta_E$ (dark shaded region) and moderate deviations with $\Delta\delta \geq 0.03\theta_E$ (light shaded region). The angular Einstein ring radius of a Galactic bulge event caused by a stellar mass lens with $m \sim 0.3 M_\odot$ located midway between the observer and the source, i.e. $D_{OL}/D_{OS} = 0.5$, is $\theta_E \sim 550 \mu\text{-arcsec}$. For this event, the deviations in these regions respectively are $\Delta\delta \gtrsim 50 \mu\text{-arcsec}$ and $\Delta\delta \gtrsim 15 \mu\text{-arcsec}$. In Figure 2 and 3, we present the light and astrometric curves of the events resulting from the source trajectories marked in the map (long straight lines with arrows). The assumed planetary separation is $u_p = 1.2$ and the planet/primary mass ratio is $q = 10^{-3}$, which is roughly equivalent to the mass ratio between the Jupiter and the Sun. To show how the astrometric deviation is correlated to the photometric one, we also present the excess magnification map (the contour map in the second panel of Fig. 1) and the curves of ϵ and $\Delta\boldsymbol{\delta}$ around the time and near the region of significant deviations (Figure 4). The contours of the excess magnification map are drawn at the levels of $\epsilon = -10\%$, -5% , 5% , and 10% and the regions of positive excesses are distinguished by grey-scales.

From the analysis of the figures, we find the following properties of $\Delta\boldsymbol{\delta}$ induced by planets with separations from the primary larger than θ_E .

(i) The most significant astrometric deviations ($\Delta\delta \gtrsim 0.1\theta_E$) occur in the region near the caustics and also in the region close to the primary-planet axis between the two caustics. Since the planetary caustic for this system is located on the planet side with respect to the center of mass, the major deviation region is also located on the planet side. The biggest deviations occur when the source crosses the caustics (e.g., the event caused by the source trajectory 3). For this case, the resulting astrometric curve exhibits a sharp spike due to the sudden shift of the centroid (see the corresponding $\boldsymbol{\delta}$ and $\Delta\boldsymbol{\delta}$ of the event in Fig. 3 and 4).[†] Even for non-caustic crossing events, however, significant deviations can also occur if the source trajectory passes through the primary-planet axis region between the central and

[†] For more detailed discussion about the behavior of $\Delta\boldsymbol{\delta}$ for caustic crossing events, see § 3.3 of Han (2000).

planetary caustics. For this case, the deviation is smooth as shown in Fig. 3 and the right panels of Fig. 4.

(ii) The deviation vectors in most of the major deviation region are directed towards the planet along the primary-planet axis. As a result, a majority of the events caused by a planetary lens system with $u_p > 1.0$ will have major deviations oriented towards the planet. The only exception occurs if the source passes through the small region on the opposite side of the primary lens (e.g., the event caused by the source trajectory 6), within which the major deviation vector is directed away from the planet.

(iii) As the distance from the primary-planet axis increases, the amount of deviation decreases. In addition, the direction of $\Delta\boldsymbol{\delta}$ is reversed compared to that of $\Delta\boldsymbol{\delta}$ in the major deviation region. Since the major deviation region is surrounded by the region of moderate deviations, the astrometric curve of a typical event with significant deviations will have smaller deviations with an opposite orientation to that of the major deviation vectors before and after the major deviation. We note that planet-induced photometric deviations also exhibit a similar property, i.e. having smaller deviations with an opposite sign of ϵ around the major deviation (Gaudi & Gould 1992).

(iv) The photometric and astrometric deviations are closely correlated, as discussed by Safizadeh et al. (1999). From the comparison of the sizes between the photometric and the corresponding astrometric deviations, one finds that the amount of $\Delta\boldsymbol{\delta}$ increases as $|\epsilon|$ increases. From the comparison of the sign of ϵ and the direction of $\Delta\boldsymbol{\delta}$, one also finds that $\Delta\boldsymbol{\delta}$ is directed towards the planet when $\epsilon > 0$ (positive deviation) and vice versa. Since the major astrometric deviation vectors of the events caused by this type of lens system are usually directed towards the planet, the light curves of these events are more likely to have positive major deviations (see Fig. 2 and the right panels of Fig. 4). The location of the major astrometric deviation regions and the orientations of $\Delta\boldsymbol{\delta}$ in this region can be understood from the correlations between $\Delta\boldsymbol{\delta}$ and ϵ . The most significant photometric deviations occur when the source is located near the primary-planet axis because at this moment the images are located near the axis and approaches most closely the planet (Gould & Loeb 1992). As a result, the region of major astrometric deviations is located along the axis and $\Delta\boldsymbol{\delta}$ in this region is directed also along the axis. In addition, the similarity in the properties of moderate size deviations between the astrometric and photometric perturbations around the major deviations mentioned above can also be understood from the correlations between $\Delta\boldsymbol{\delta}$ and ϵ .

4.2 Planets with $u_p < 1.0$

The lens system composed of a planet with $u_p < 1.0$ also has a single central caustic, but it has *two* planetary caustics, which are located on the *opposite* side of the planet with respect to the center of mass. Unlike the planetary caustic of the planetary lens system with $u_p > 1.0$, the planetary caustics of this lens system are *not* located on the primary-planet axis, although they are symmetric with respect to the axis (Griest & Safizadeh 1998).

In the upper panel of Figure 5, we present the map of $\Delta\boldsymbol{\delta}$ for a planetary lens system with $u_p = 0.8$ and $q = 10^{-3}$ and it is compared to the excess magnification map presented in the second panel. Also presented in Figure 6 and 7 are the light and astrometric curves of several example events resulting from the source trajectories marked in the upper panel of Fig. 5. In Figure 8, we present the photometric and astrometric deviations around the time and near the region of significant deviations for these events. From the investigation of the properties of $\Delta\boldsymbol{\delta}$ induced by the planet with $u_p < 1.0$ and comparison to those of the deviation vectors induced by the planet with $u_p > 1.0$, we find the following similarities and differences.

(i) For this system, the most significant deviations also occur near the caustic regions

and the region close to the primary-planet axis between the two types of caustics. However, since the planetary caustics are located on the opposite side of the planet with respect to the center of mass, the significant deviation regions are also located on the opposite side of the planet.

(ii) In addition, besides the small areas around the planetary caustics, $\Delta\boldsymbol{\delta}$ in most of the major deviation region are directed away from the planet along the primary-planet axis (see Fig. 7 and right panels of Fig. 8).

(iii) Similar to the behaviors of $\Delta\boldsymbol{\delta}$ induced by the planet with $u_p > 1.0$, the major deviation region is surrounded by the region of moderate deviations, within which the direction of $\Delta\boldsymbol{\delta}$ is reversed to that of $\Delta\boldsymbol{\delta}$ in the major deviation region.

(iv) The relation between the astrometric and photometric deviations is also similar to the case of the planetary system with $u_p > 1.0$; the amount of astrometric deviation increases as $|\epsilon|$ increases and its direction points towards the planet when the light curve has a positive deviation and vice versa. Because the major astrometric deviations induced by this type of planets are usually directed towards the opposite side of the planet, the light curves have negative deviations ($\epsilon < 0$) with the same probability.

(v) Another interesting finding is that most of the major planet-induced astrometric deviations point *away* from the opening of the astrometric ellipse regardless of the planetary separation (see Fig. 3 and 7).

5 VARIATIONS

In this section, we investigate the variation of the excess centroid shift patterns with the planetary separation and the planet/primary mass ratio. For this, we present excess centroid shift maps of lens systems with various values of u_p and q . In addition, to examine the effect of finite source size on the pattern of $\Delta\boldsymbol{\delta}$, we present maps of an example lens system expected for different source sizes.

In Figure 9, we present the locations of significant astrometric deviation regions for lens systems with various values of u_p . In the following Figures 10 and 11, we present the vector field maps of $\Delta\boldsymbol{\delta}$ of the corresponding lens systems in the regions around the significant deviations. The tested lens systems have a common mass ratio of $q = 10^{-3}$ and a variety of planetary separations of $u_p = 2.0, 1.7, 1.5, 1.3$ (whose maps are presented in Fig. 10), 1.0, 0.9, 0.7, and 0.5 (whose maps are presented in Fig. 11). One finds that similar to photometric deviations (Gould & Loeb), the size of significant deviation regions is maximized when $u_p \sim 1.0$ and becomes smaller as the separation increases or decreases from this value. We note, however, that the general patterns of $\Delta\boldsymbol{\delta}$ described in § 4.1 and § 4.2 still apply.

In Figure 12 and 13, we present the excess centroid shift maps of lens systems with various values of planet/primary mass ratios. The tested systems have a common planetary separation of $u_p = 1.3$ and various mass ratios of $q = 10^{-2}, 5 \times 10^{-3}, 3 \times 10^{-3}, 10^{-3}$ (whose maps are presented in Fig. 12), $5 \times 10^{-4}, 10^{-3}, 5 \times 10^{-5}$, and 10^{-5} (whose maps are presented in Fig. 13). One finds that the location of the major astrometric deviation region does not vary with mass ratio, but the size of the region decreases rapidly as q decreases. This property is also similar to that of photometric deviations.

In Figure 14, we presented the excess centroid shift maps of a common lens system (with $u_p = 1.2$ and $q = 10^{-3}$) but with different source sizes. Considering the finite source effect, the position of the image centroid is given by

$$\boldsymbol{\theta}_c = \frac{\int I(\mathbf{r}) A_p(\mathbf{r}) \theta_{c,p}(\mathbf{r}) d^2r}{\int I(\mathbf{r}) A_p(\mathbf{r}) d^2r} \quad (10)$$

where $I(\mathbf{r})$ is the surface intensity distribution of the source star and \mathbf{r} represents the displacement vector of an area element on the source star surface with respect to the lens.

For the construction of the maps, we assume the distribution of the source star surface intensity is uniform. We note that $\Delta\boldsymbol{\delta}$ in the maps are the deviations from the centroid shifts of the single primary lens which are also affected by the finite source effect. When a single lens event is affected by the finite source effect, the resulting centroid shift trajectory is no longer an ellipse (Mao & Witt 1998). We test three different source sizes of $\varrho_* = 0.005\theta_E$, $0.01\theta_E$, and $0.05\theta_E$. From the figure, one finds that the detailed structure of $\Delta\boldsymbol{\delta}$ is smeared out with the increasing source size, as pointed out by Safizadeh et al. (1998). For example planetary microlensing astrometric curves affected by the finite source effect, see Fig. 3 of Safizadeh et al. (1998).

6 CONCLUSION

We investigate the astrometric properties of planet-induced deviations in the trajectory of the microlensed source star's centroid shift motion. For this purpose, we construct maps of excess centroid shifts from which one can obtain an overview about the behaviors of $\Delta\boldsymbol{\delta}$ of all events without testing their individual centroid shift trajectories. From the analysis of the maps for various types of lens systems, we find that major astrometric deviations occur not only in the region around caustic but also in the region close to the primary-planet axis between caustics. The region of major deviations is surrounded by the region of moderate deviations in which the orientation of $\Delta\boldsymbol{\delta}$ is reversed compared to that in the major deviation region. Due to the difference in the locations of the caustics between the planetary lens systems with $u_p > 1.0$ and $u_p < 1.0$, the locations of the major deviations and the orientations of $\Delta\boldsymbol{\delta}$ within these regions of the two types of lens systems are different from each other. From the investigation of the correlations between the astrometric and photometric deviations, we find that both the size and the direction of the astrometric deviation are closely related to the magnitude and sign of the photometric deviation, as discussed by Safizadeh et al. (1998). By investigating the variation of the pattern of $\Delta\boldsymbol{\delta}$ with the planetary separation, planet/primary mass ratio, and source size, we find the astrometric and photometric deviations both have similar dependence upon these parameters.

We would like to thank K. Griest for making useful comments about the paper. This work was supported by a grant (Basic Research Fund) of the Korea Science & Engineering Foundation (KOSEF).

REFERENCES

Alard C., Guibert J., 1997, A&A, 326, 1
 Albrow M. D., et al., 1998, ApJ, 509, 684
 Alcock C., et al. 1993, Nat, 365, 621
 Aubourg E., et al., 1993, Nat, 365, 623
 Boden A. F., Shao M., Van Buren D., 1998, ApJ, 502, 538
 Bolatto A. D., Falco E. E., 1994, ApJ, 436, 112
 Bond I., 2000, in ASP Conf. Proc. Microlensing 2000: A New Era of Microlensing Astrophysics, eds. J. W. Menzies and P. D. Sackett, in press
 Bozza V., 1999, A&A, 348, 311
 Colavita M. M., et al., 1998, Proc. SPIE, 3350-31, 776
 Gaudi B. S., Gould A., 1997, ApJ, 486, 85
 Gaudi B. S., Sackett P. D., 2000, ApJ, 528, 56
 Gould A., Loeb A., 1992, ApJ, 396, 104
 Griest A., Safizadeh N., 1998, ApJ, 500, 37
 Han C., 2001, MNRAS, 325, 1281
 Høg E., Novikov I. D., Polnarev A. G., 1995, A&A, 294, 287
 Jeong Y., Han C., Park S.-H., 1999, ApJ, 511, 569
 Mao S., Paczyński B., 1991, ApJ, 374, L37
 Mao S., Witt H. J., 1998, MNRAS, 300, 1041
 Mariotti J. M., et al., 1998, Proc. SPIE, 3350-33, 800
 Miralda-Escudé J., 1996, ApJ, 470, L113
 Miyamoto M., Yoshii Y., 1995, AJ, 110, 1427

Paczyński B., 1986, *ApJ*, 304, 1
Paczyński B., 1998, *ApJ*, 494, L23
Rhie, S. H., et al., 2000, *ApJ*, 533, 378
Safizadeh N., Dalal N., Griest K., 1999, *ApJ*, 522, 512
Udalski A., Szymański M., Kaluzny J., Kubiak M., Krzemieński W., Mateo M., Preston G. W., Paczyński B., 1993, *Acta Astron.*, 43, 289
Unwin S., Boden A., Shao M., 1997, in *AIP Conf. Proc. 387, Space Technology and Applications International Forum 1997*, ed. M. S. El-Genk (New York: AIP), 63
Walker M. A., 1995, *ApJ*, 453, 37
Wambsganss J., 1997, *MNRAS*, 384, 172
Witt H. J., Mao S., 1995, *ApJ*, 447, L105

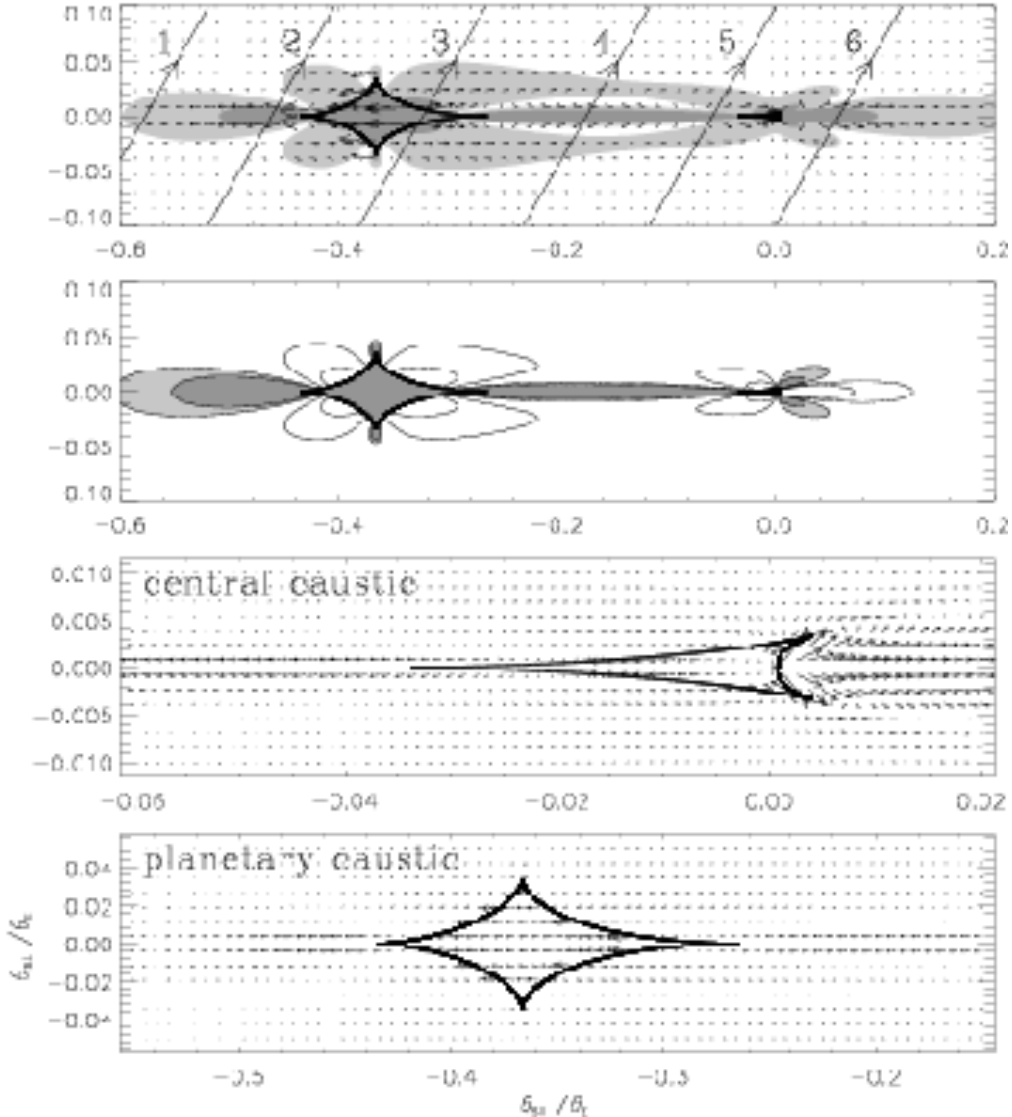


Figure 1. The vector field map of the excess centroid shift $\Delta\delta$ of an example planetary lens system with a planetary separation $u_p = 1.2$ and a mass ratio $q = 10^{-3}$. The positions are selected so that the center of mass is at the origin and $(\theta_{S\parallel}, \theta_{S\perp})$ represent the components of the source position that are parallel and normal to the primary-planet axis. Both the primary and the planet are located on the $\theta_{S\parallel}$ axis and the planet is to the left. The two closed figures drawn by thick solid lines represent the caustics. Grey-scales are used to represent the regions of significant deviations with $\Delta\delta \geq 0.1\theta_E$ (dark shaded region) and moderate deviations with $\Delta\delta \geq 0.03\theta_E$ (light shaded region). The long straight lines with arrows represent the source trajectories of the events whose resulting light and astrometric curves are presented in Fig. 2 and 3, respectively. Second panel: The contour map of the excess magnification for the same lens system. The contours are drawn at the levels of $\epsilon = -10\%, -5\%, 5\%, 10\%$. The region of positive excesses are distinguished by grey-scales. Lower two panels: Blow-ups of the excess centroid shift map in the regions around the central (third panel) and planetary caustics (last panel).

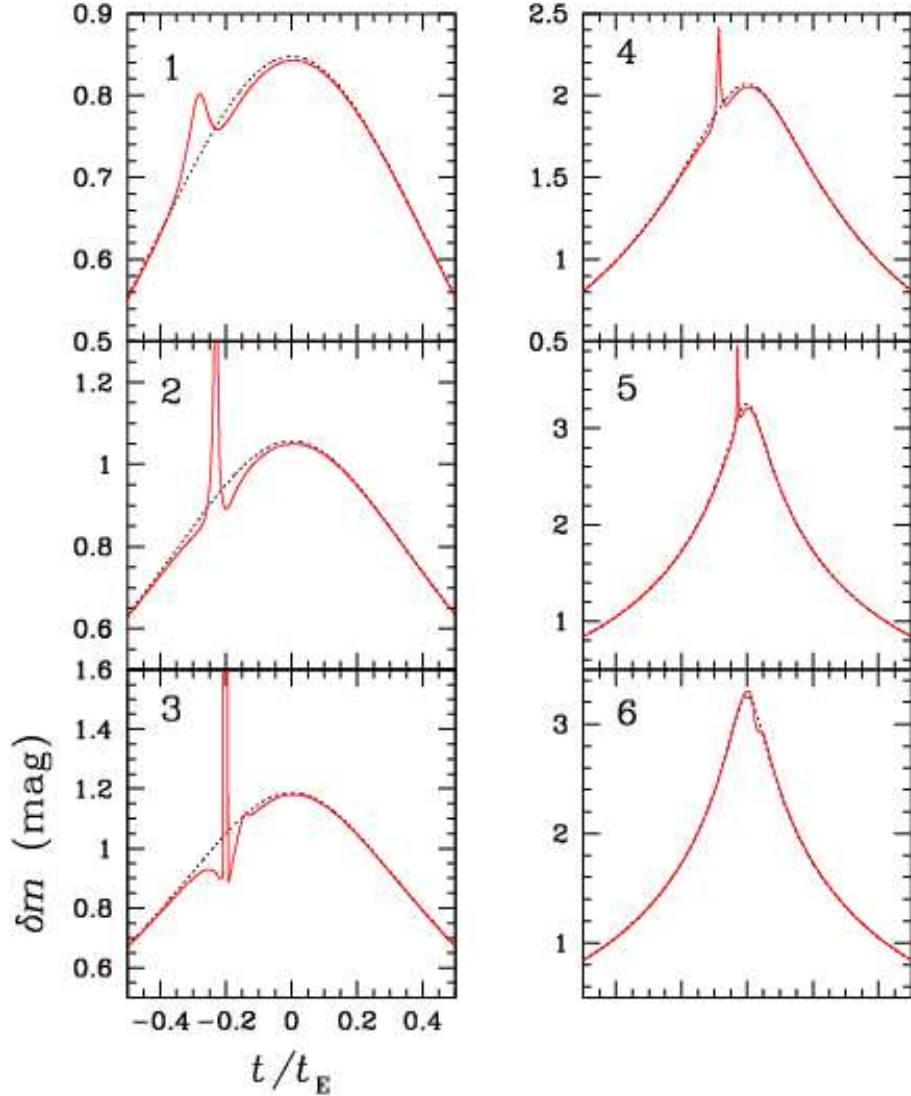


Figure 2. The light curves of the events resulting from the source trajectories marked in the upper panel of Fig. 1. The number in each panel corresponds to the trajectory number marked in Fig. 1. The dotted curves represent the single lens event light curves that are expected in the absence of the planet.

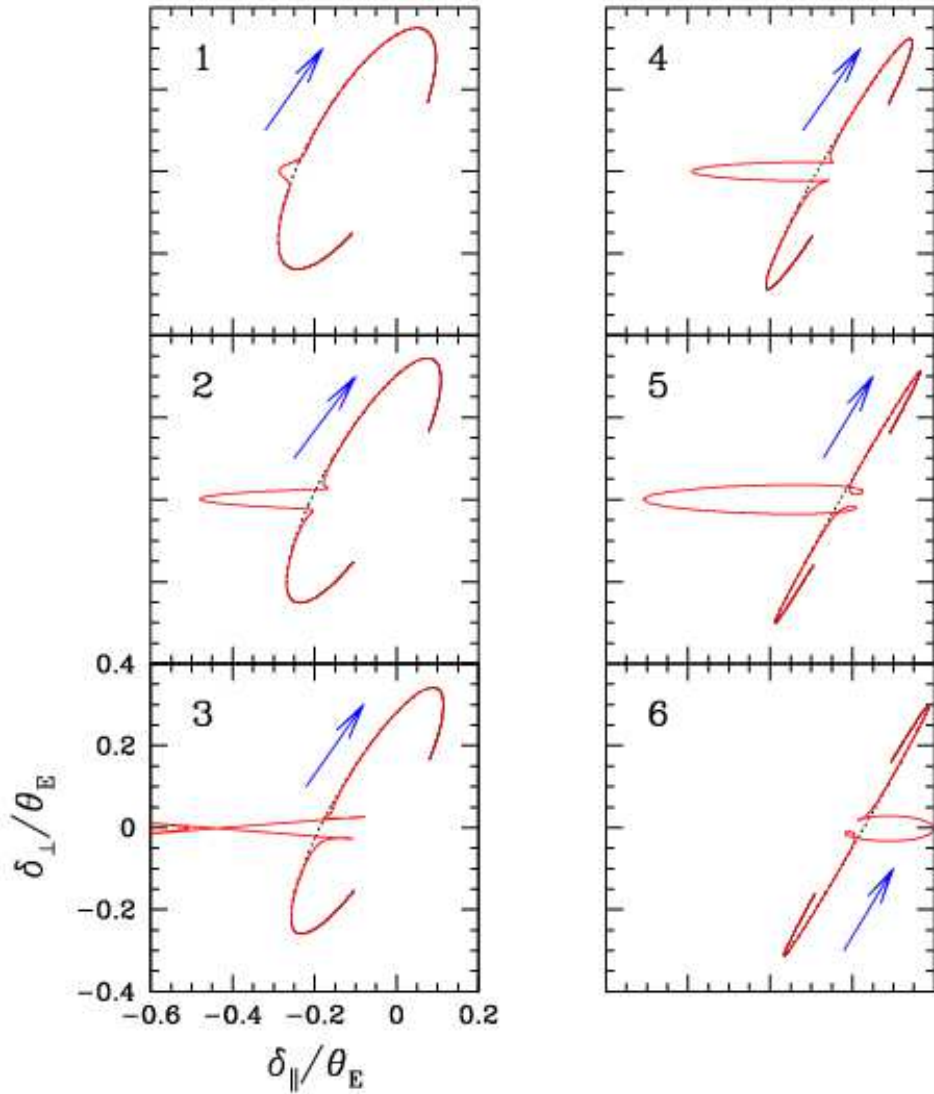


Figure 3. The astrometric curves of the events resulting from the source trajectories marked in the upper panel of Fig. 1. The dotted curves represent the astrometric curves expected in the absence of the planet. $(\delta_{\parallel}, \delta_{\perp})$ are the components of δ that are parallel and normal to the primary-planet axis and the arrow represents the direction of the centroid motion.

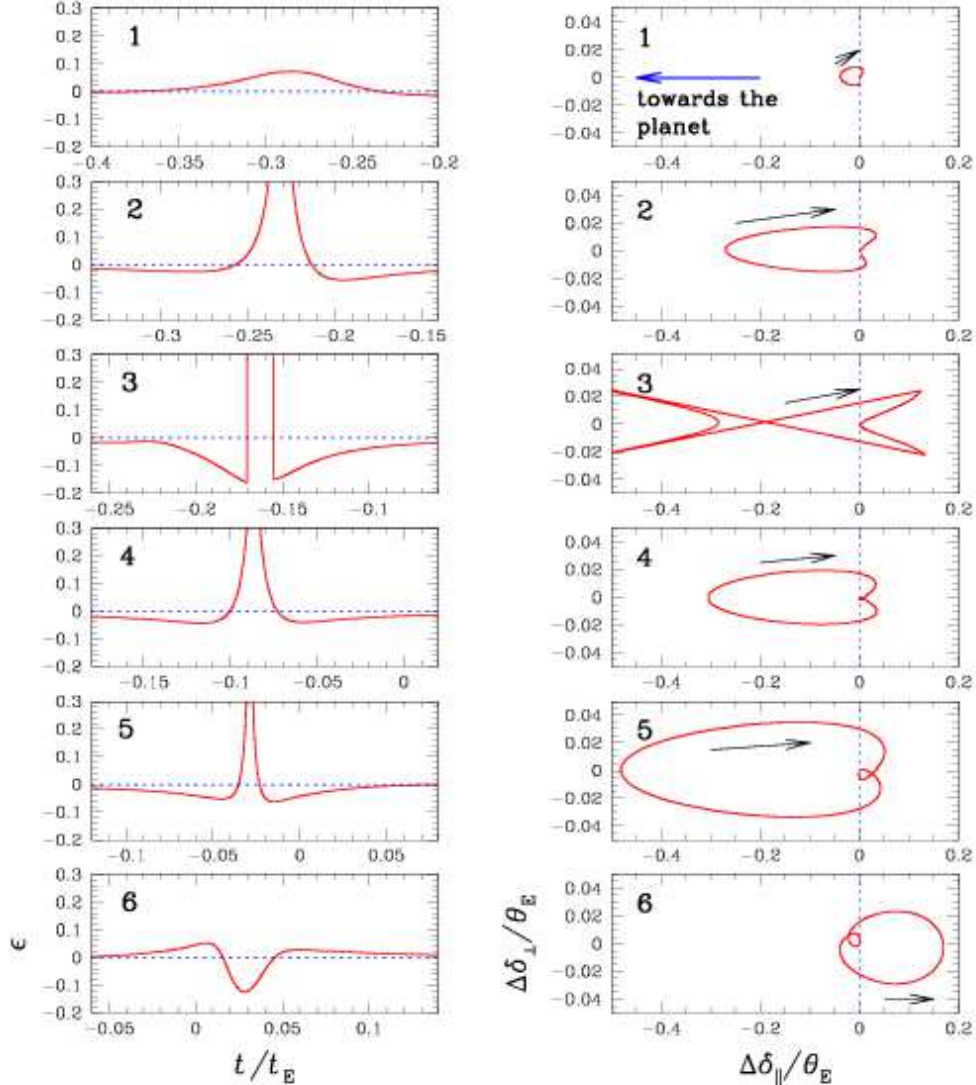


Figure 4. The excess magnification ϵ (left panels) and the excess centroid shift vector $\Delta\delta$ (right panels) around the time and near the region of significant deviations for the events resulting from the source trajectories marked in Fig. 1. The number in each panel corresponds to the trajectory number. Note that the abscissa and ordinate of $\Delta\delta$ are arbitrarily scaled.

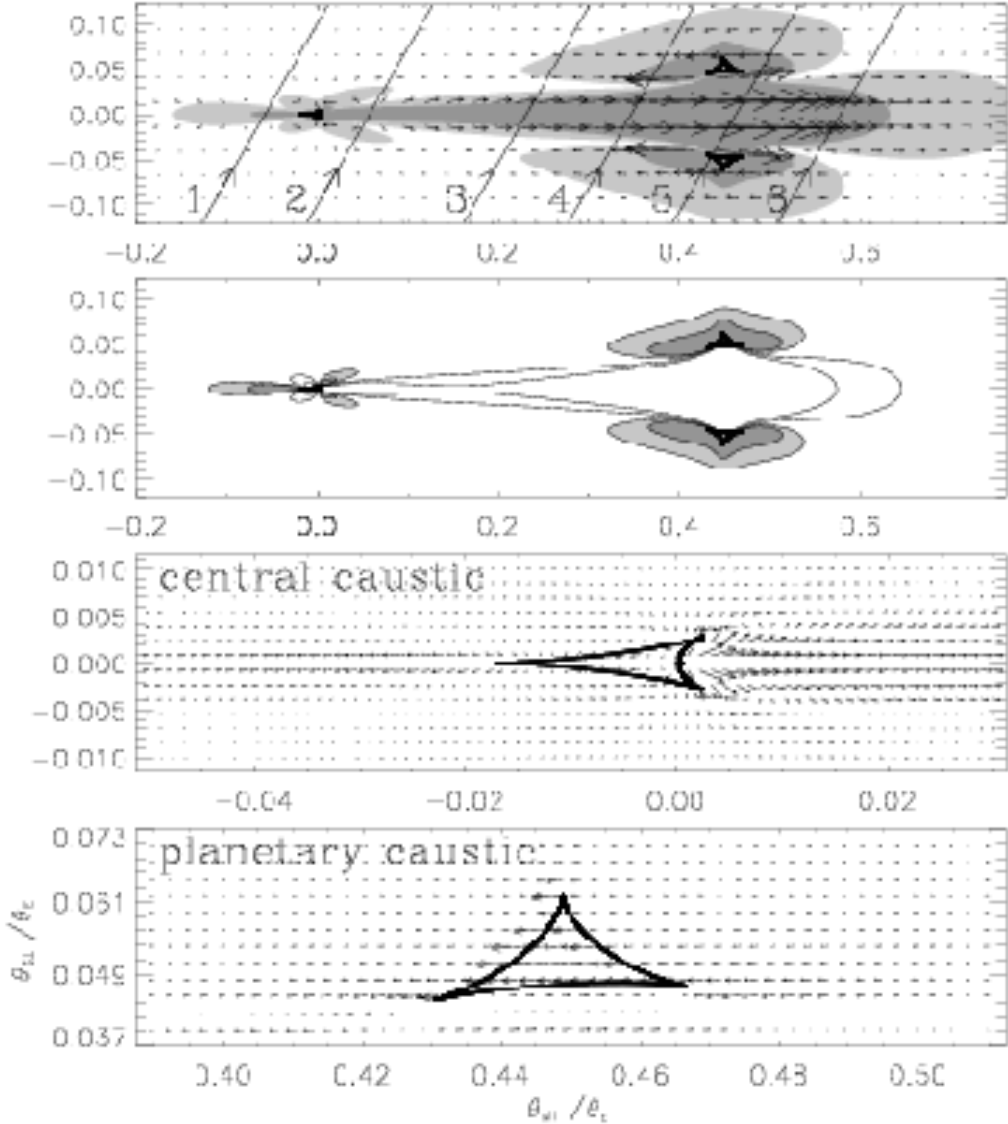


Figure 5. The vector field map of $\Delta\delta$ (upper panel) and the contour map of ϵ (second panel) of an example planetary lens system with $u_p = 0.8$ and $q = 10^{-3}$. The lower two panels are the blow-ups of the the excess centroid shift map in the region around caustics. Notations are same as in Fig. 1.

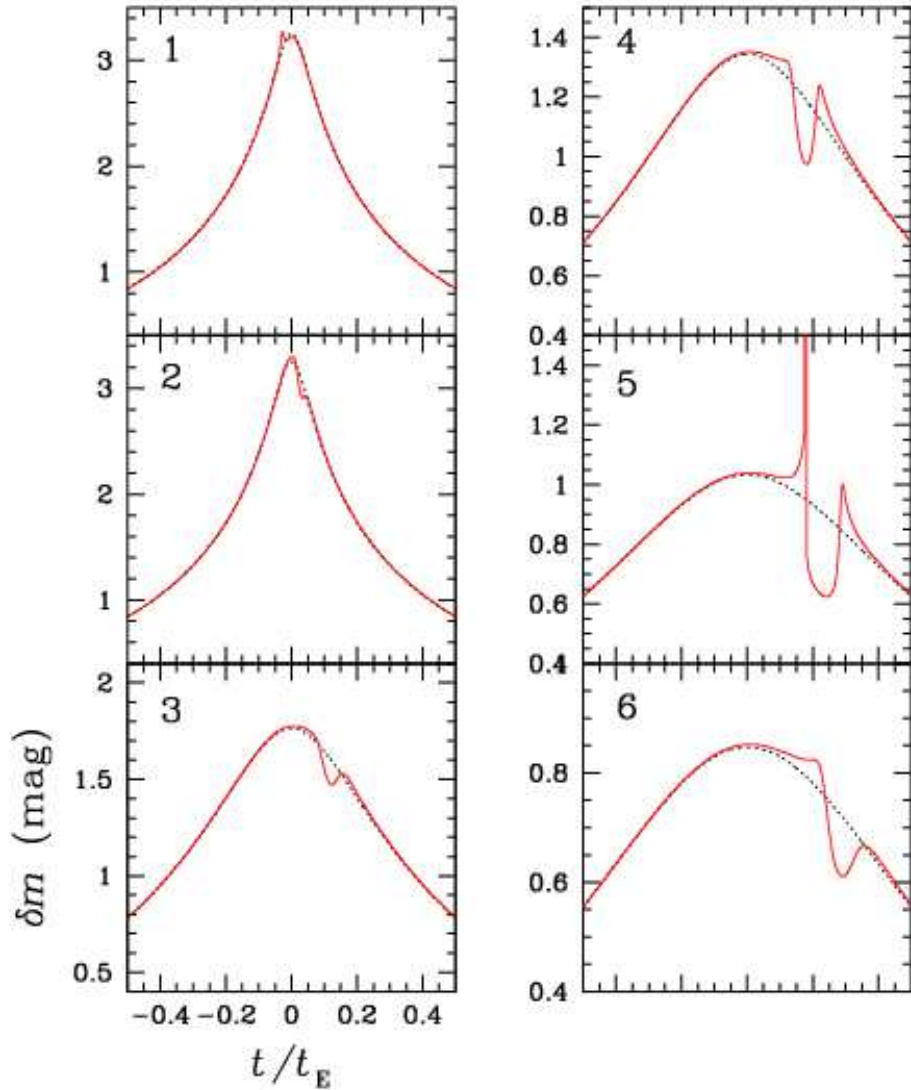


Figure 6. The light curves of the events resulting from the source trajectories marked in the upper panel of Fig. 5. Notations are same as in Fig. 2.

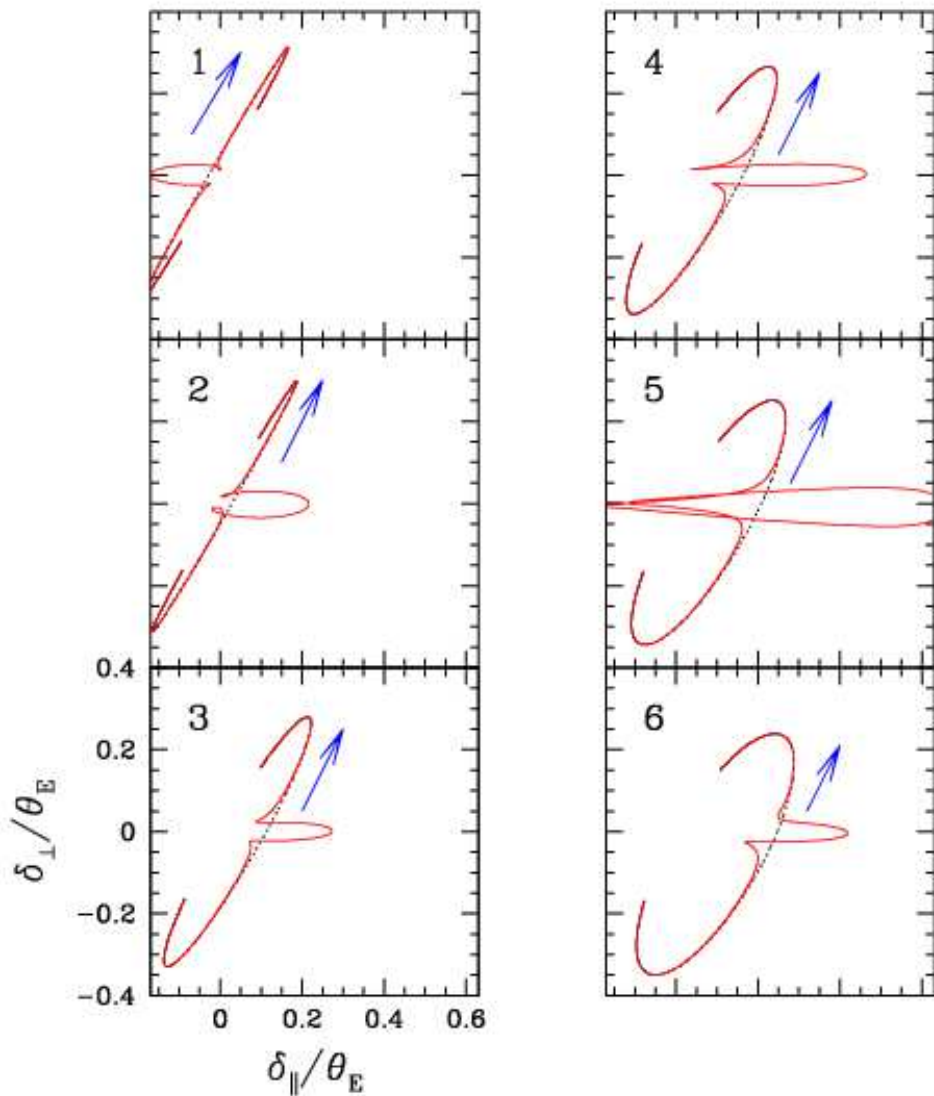


Figure 7. The astrometric curves of the events resulting from the source trajectories marked in the upper panel of Fig. 5. Notations are same as in Fig. 3.

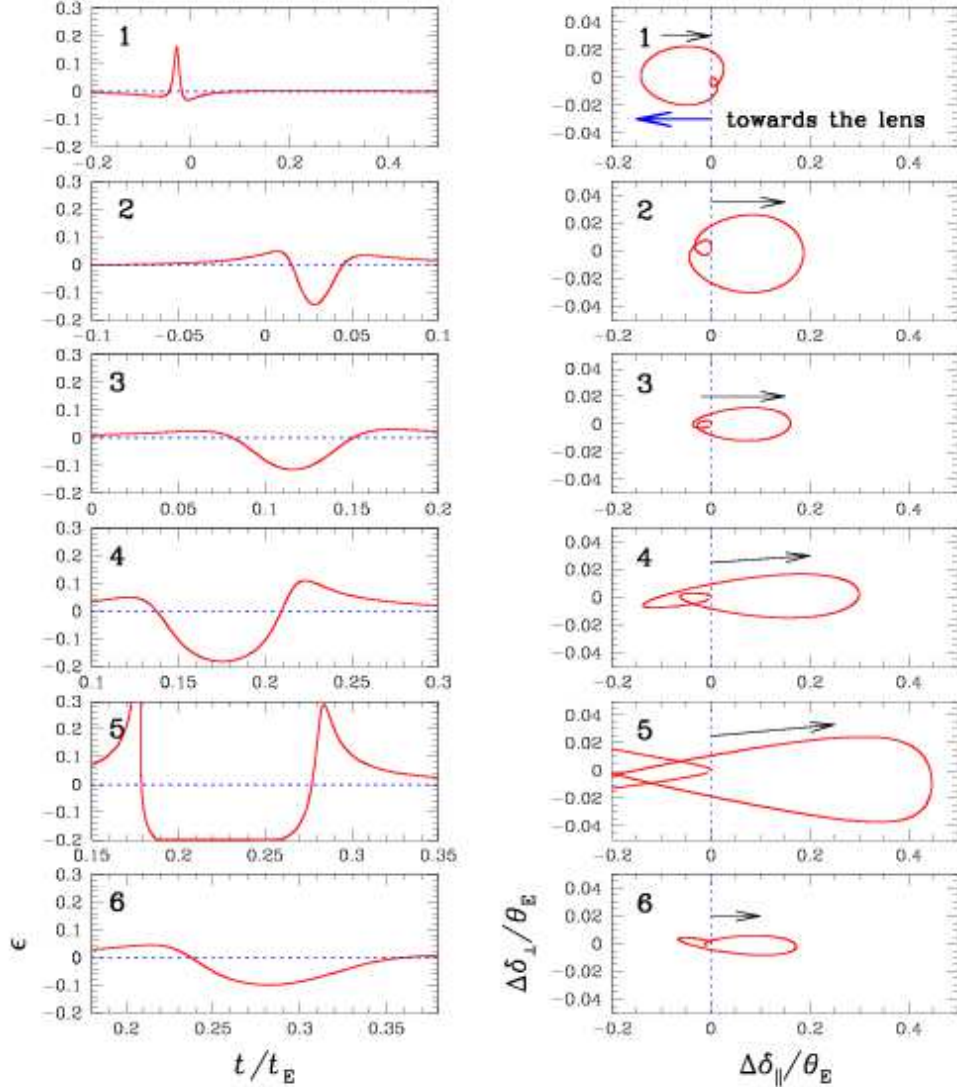


Figure 8. The excess magnification ϵ (left panels) and the excess centroid shift vector $\Delta\delta$ (right panels) for the events resulting from the source trajectories marked in Fig. 5. Notations are same as in Fig. 4.

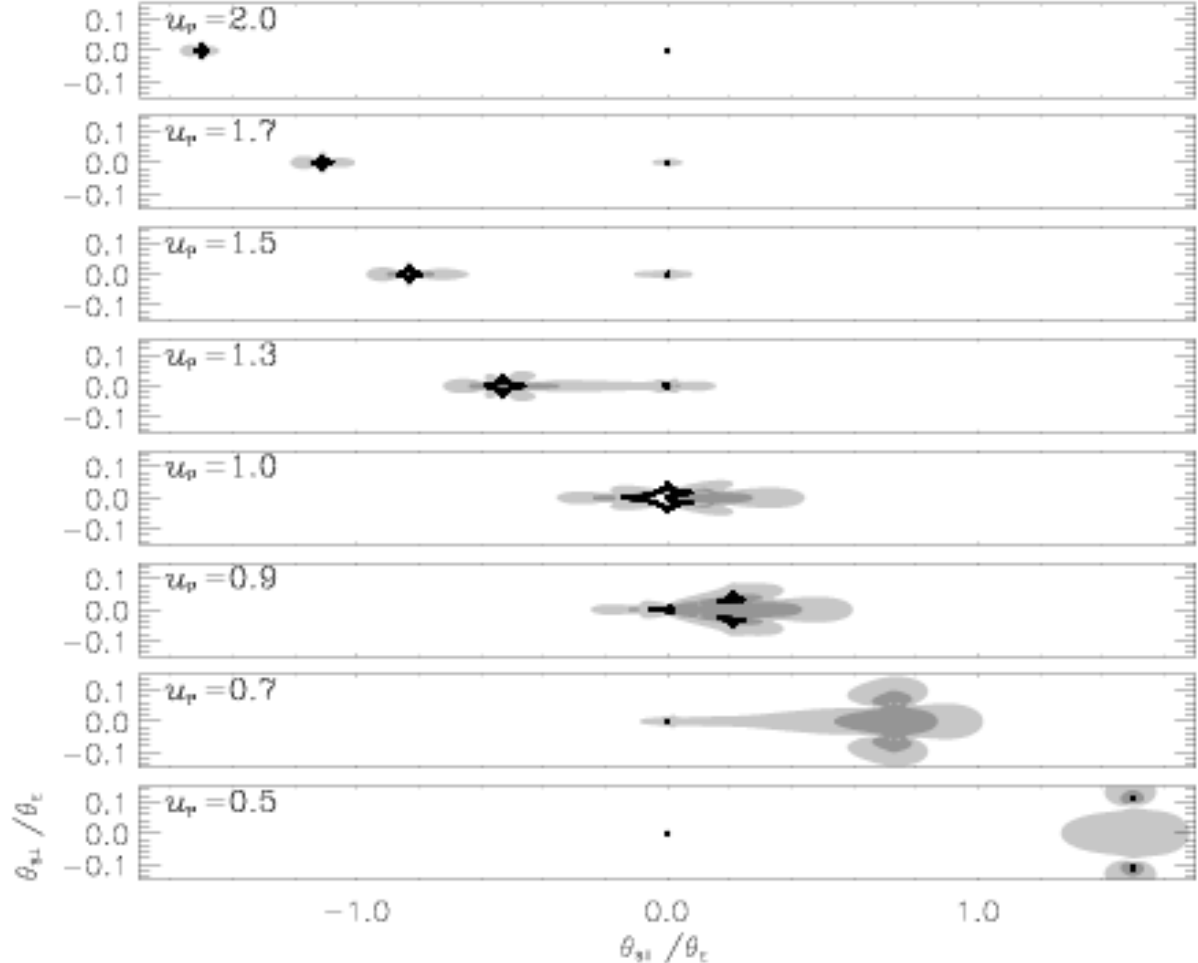


Figure 9. Variation of the locations of significant astrometric deviation regions with planetary separation u_p . The light and dark shades are used to represent the regions with $\Delta\delta \geq 0.03\theta_E$ and $\Delta\delta \geq 0.1\theta_E$, respectively. The lens systems have a common mass ratio of $q = 10^{-3}$. The vector field maps of $\Delta\delta$ of the individual lens systems are presented in the following Fig. 10 and 11.

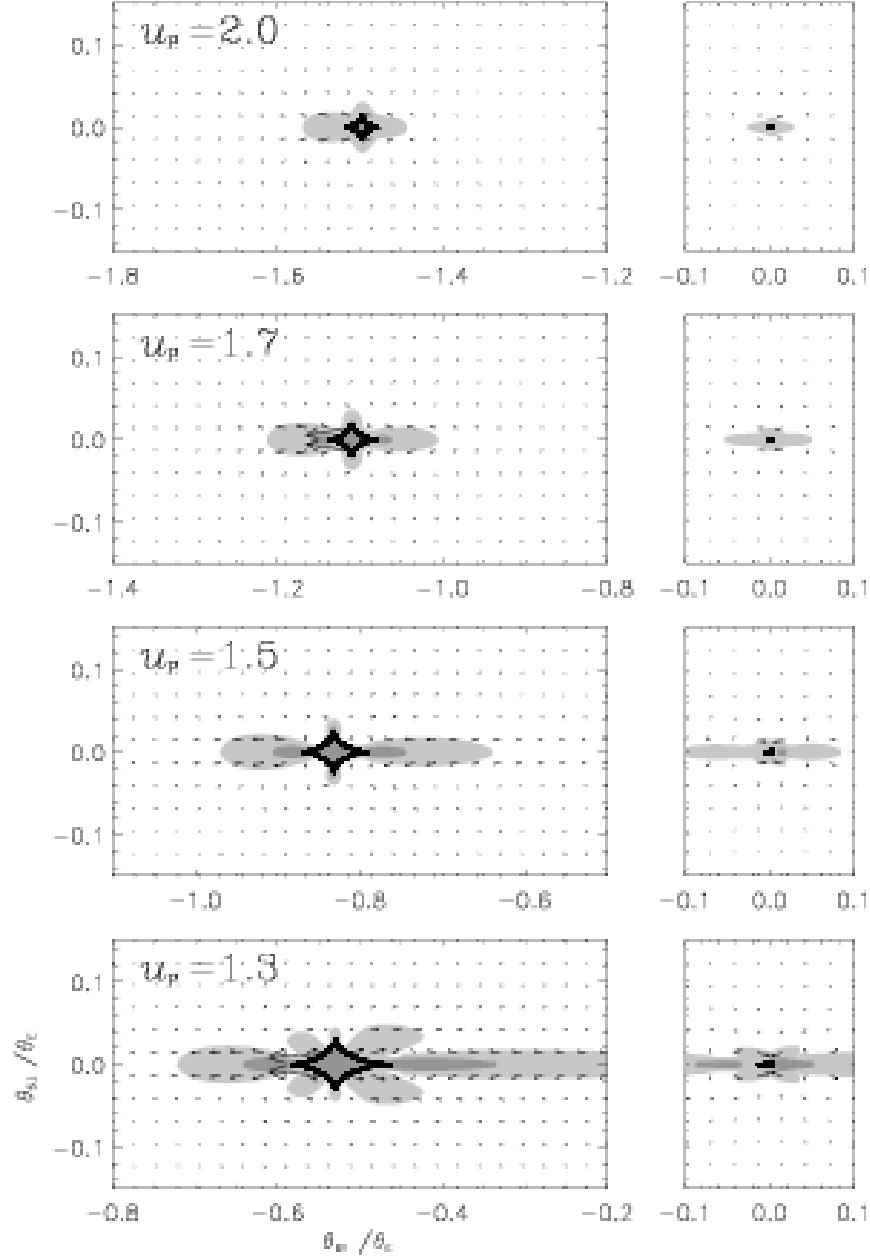


Figure 10. Variation of the vector field map of $\Delta\delta$ with the planetary separation u_p . The lens systems have a common mass ratio of $q = 10^{-3}$. Notations are same as in the upper panel of Fig. 1.

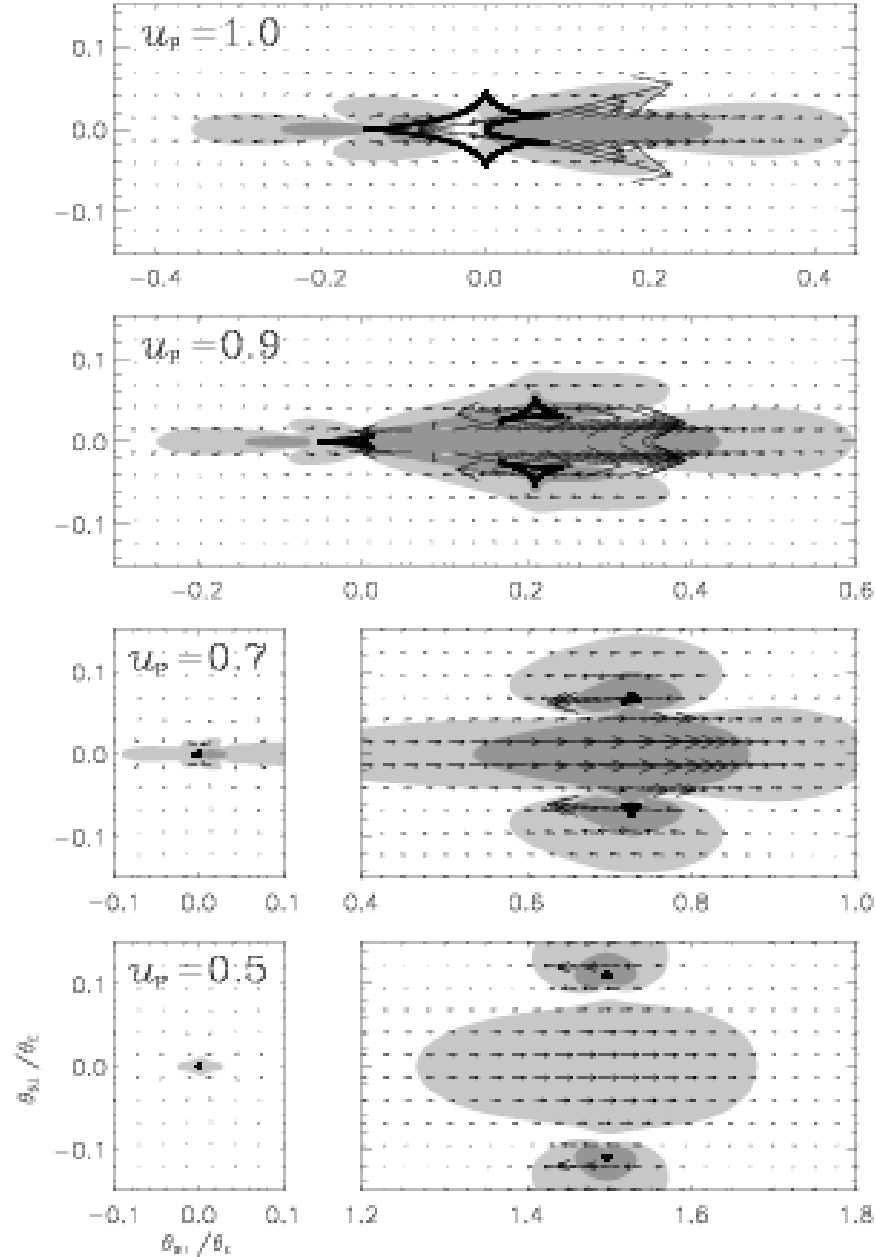


Figure 11. Variation of the vector field map of $\Delta\delta$ with the planetary separation u_p . The maps are similar to those presented in Fig. 10, but for lens systems with smaller planetary separations.

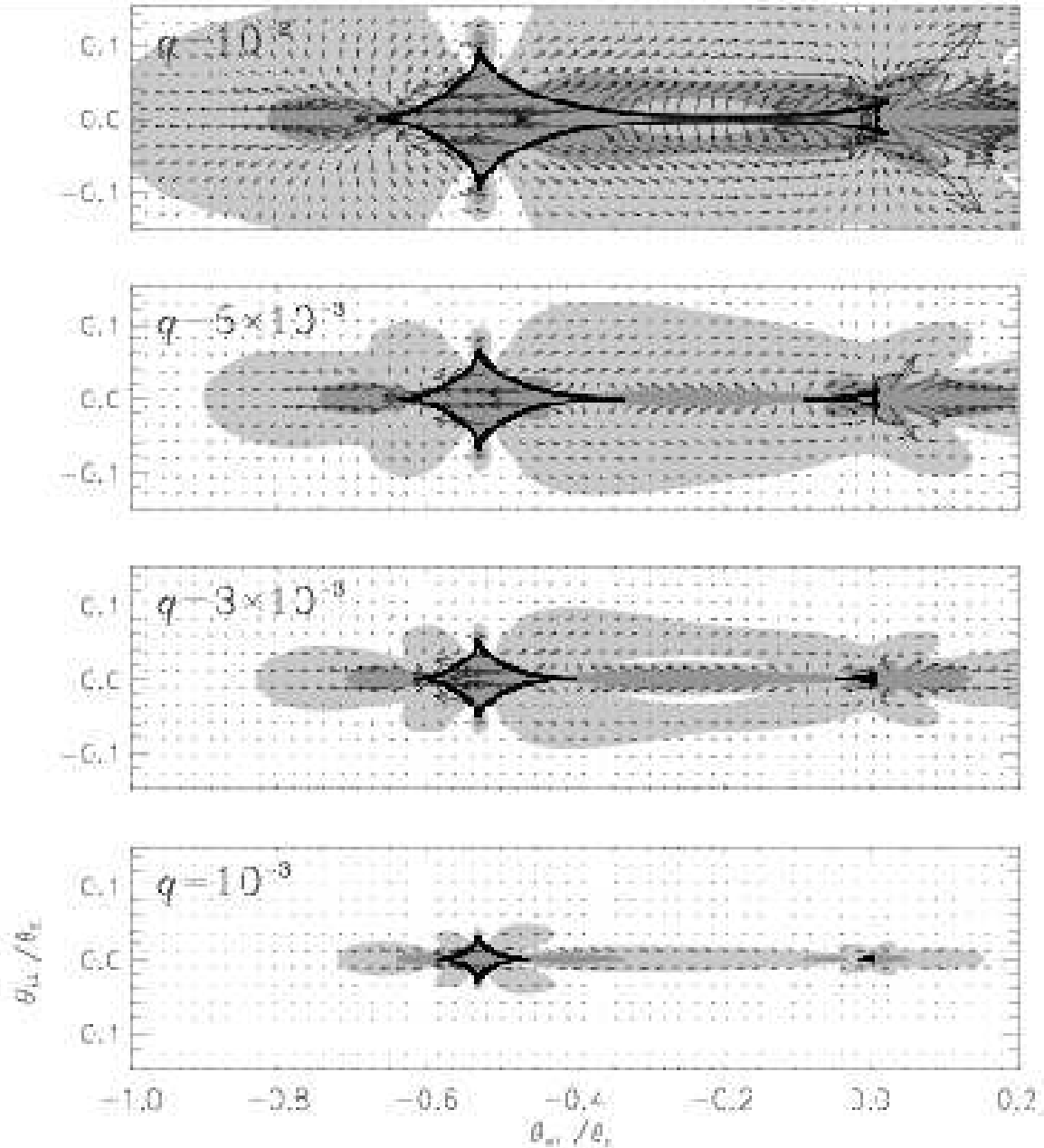


Figure 12. Variation of the vector field map of $\Delta\delta$ with the planet/primary mass ratio q . The lens systems have a common planetary separation of $u_p = 1.3$. Notations are same as in the upper panel of Fig. 1.

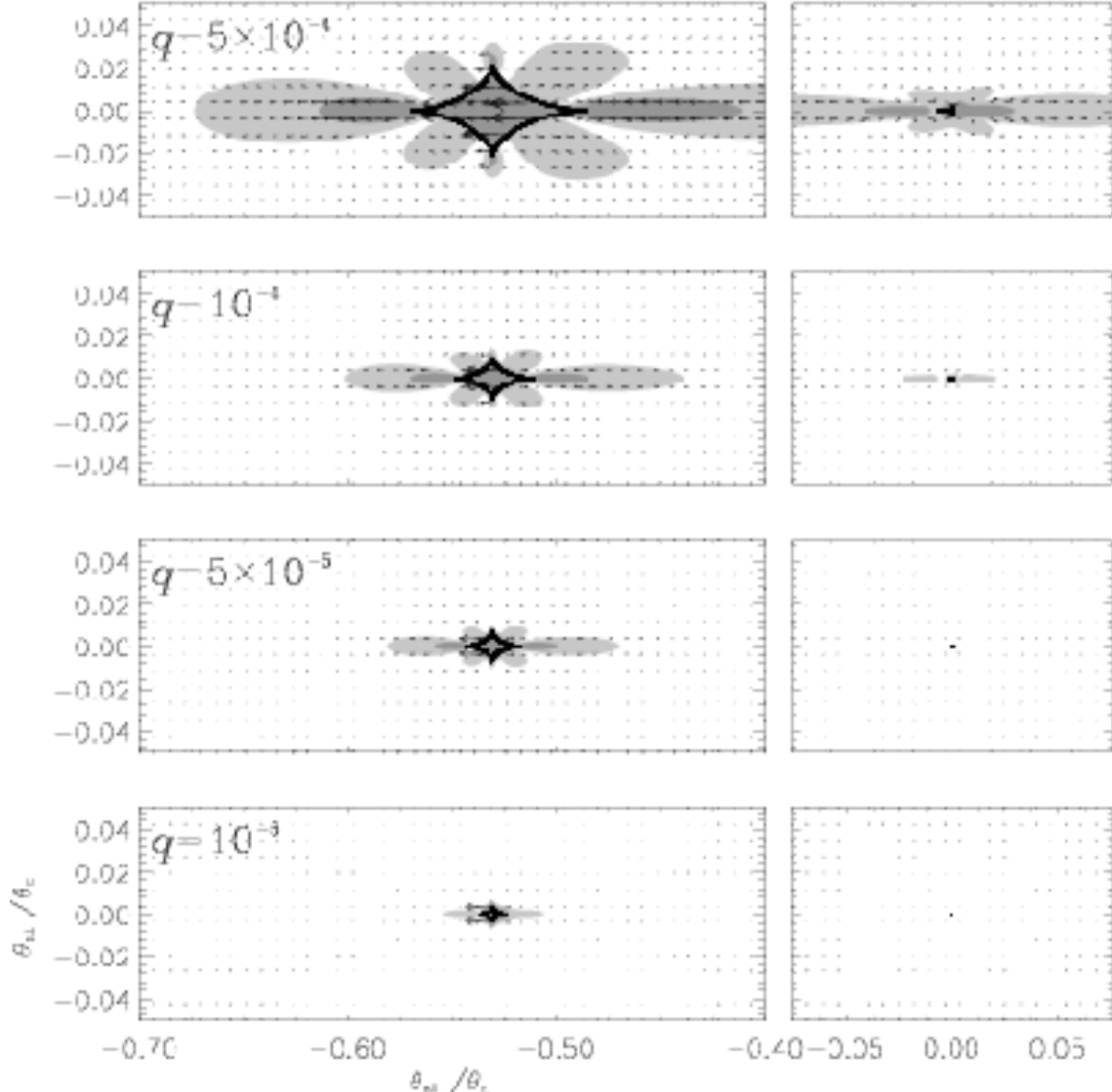


Figure 13. Variation of the vector field map of $\Delta\delta$ with the planet/primary mass ratio q . The maps are similar to those presented in Fig. 12, but for lens systems with smaller mass ratios. Note that the scale of the maps are different from that of the maps presented in Fig. 12.

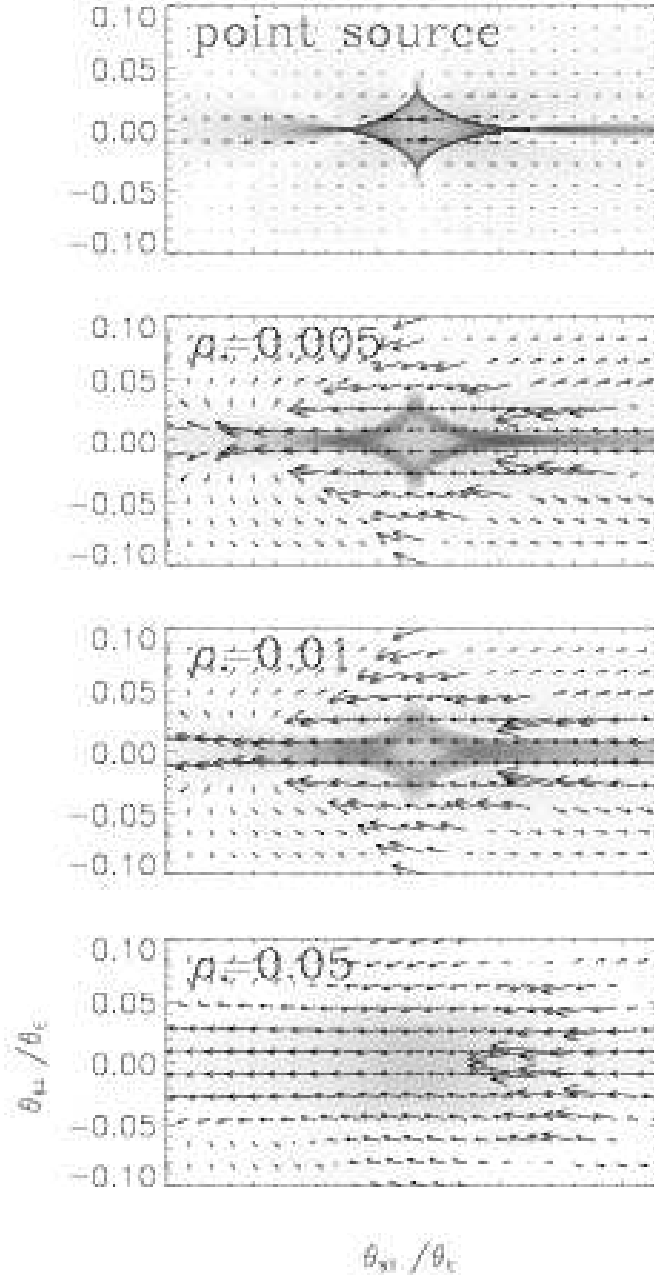


Figure 14. Variation of the vector field map of $\Delta\delta$ with source size. Unlike other maps, we do not draw caustics on these maps to better show the detailed structures near the caustics. We draw 60 grey-scales in the range of $\Delta\delta = 0.03\theta_E - 0.7\theta_E$.